

Investigating Hydroxide Anion Interfacial Activity by Classical and Multistate Empirical Valence Bond Molecular Dynamics Simulations

Collin D. Wick^{*,†} and Liem X. Dang^{‡,§}

Louisiana Tech University, Ruston, Louisiana 71270, and Pacific Northwest National Laboratory, Richland, Washington 99352

Received: January 12, 2009; Revised Manuscript Received: March 19, 2009

Molecular dynamics simulations were carried out to understand the propensity of the hydroxide anion for the air–water interface. Two classes of molecular models were used, a classical polarizable model and a polarizable multistate empirical valence bond (MS-EVB) potential. The latter model was parametrized to reproduce the structures of small hydroxide–water clusters based on proton reaction coordinates. Furthermore, nuclear quantum effects were introduced into the MS-EVB model implicitly by refitting its potential energy function to account for them. The final MS-EVB model showed reasonable agreement with experiment and *ab initio* molecular dynamics simulations for dynamical and structural properties. The free-energy profiles for both the classical and MS-EVB models were mapped out across the air–water interface, and the classical model gave a higher free energy at the interface with respect to bulk. However, the MS-EVB model gave little free-energy difference between when the hydroxide anion was in the bulk and when it was present at the air–water interface with its oxygen fully solvated and its hydrogen pointing toward the vapor. When the hydroxide oxygen started to desolvate, the free energy increased dramatically, suggesting that the hydroxide anion can be found in the interfacial region.

I. Introduction

Hydroxide anions are ubiquitous in nature, and its properties are widely important in chemical, biological, environmental, and atmospheric processes.¹ In many of these cases, some of the most important chemistry occurs at the interface of water with either air or other solvents. For instance, when trace gases approach an aqueous aerosol, it initially will come into contact with the air–water interface, and the surface pH will influence the uptake of these species. If a hydroxide anion has a propensity for the air–water interface, it will signal a possibility that the surface will be more basic than the aqueous bulk, depending on the hydronium interfacial activity. For the case of hydronium ions, it is reasonably well established that they have a propensity for the air–water interface, leading to the conclusion that for acid solutions, aqueous surfaces are acidic.^{2–5} However, there is conflicting information about the propensity of the hydroxide anion for the air–water interface. Macroscopic bubble and droplet electrophoresis experiments suggest that the hydroxide anion has a propensity for the air–water, oil–water, and general apolar–water interfaces.^{6–12} Sum frequency generation (SFG) and second harmonic generation (SHG) studies of an interface between air and a NaOH concentrated aqueous solution suggested that the hydroxide anion may have a minor but not a significant presence at the air–water interface.^{13,14} Computational studies have provided conflicting information as well. For instance, the hydroxide anion was found to have a propensity for the interface between water and a hydrophobic wall using a classical nonpolarizable force field,¹⁵ but subsequent studies found that when thermal fluctuations were taken into account,

this was ameliorated.¹⁶ Also, it was found that for concentrated NaOH solutions using a classical polarizable force field, the hydroxide anion had a propensity for the interface.¹⁷ Another study, using models of similar complexity but with a modified hydroxide interaction potential, found that the hydroxide anion was repelled from the interface at very low concentrations.³ In addition, *ab initio* molecular dynamics (AIMD) and cluster studies further suggested that the hydroxide anion was repelled from the air–water interface,³ while other AIMD simulations found that both the hydroxide and hydronium had a propensity for the hydrophobic–water interface.¹⁸

There has been similar controversies related to the propensity of large soft anions for the interface,¹⁹ in which surface tension measurements promote an interface depleted of ions while molecular simulation and surface-selective spectroscopy generally promote a surface with anions present.^{20–23} There is an added challenge in understanding the propensity of hydroxide anions for the interface in comparison with simple monovalent ions, the fact that hydroxide anions can share protons with adjacent water molecules. The classical models used in the previously described simulations do not include this explicitly. It may be important to incorporate proton sharing in a molecular model to determine if it has a propensity for the air–water interface. To account for this, AIMD calculations can be employed, which have been used extensively to understand hydroxide structure and dynamics in bulk water,^{24–27} but these are very computationally demanding.

A method that can be a good compromise between classical and AIMD simulations is the multistate empirical valence bond (MS-EVB) model, which incorporates proton sharing between multiple molecules and has been used significantly to understand the hydronium ion in solution.^{28,29} For a hydroxide anion in solution, the MS-EVB model, to the knowledge of the authors, has not been applied. The fact that waters share protons with the hydroxide oxygen may be of importance for understanding

* To whom correspondence should be addressed. E-mail: cwick@latech.edu.

[†] Louisiana Tech University.

[‡] Pacific Northwest National Laboratory.

[§] E-mail: liem.dang@pnl.gov.

TABLE 1: Potential Parameters for the Flexible Water Model and Hydroxide Anion Used in the MS-EVB Potential

property	H ₂ O value	OH ⁻
D_0 (kcal/mol)	105.69	134.95
α (\AA^{-1})	2.279	2.08
r_0 (\AA)	eq 2	0.969
k_a (kcal mol ⁻¹ rad ⁻² \AA^{-1})	51.91	N/A
k_b (kcal mol ⁻¹ rad ⁻² \AA^{-2})	36.8	N/A
k_c (kcal mol ⁻¹ rad ⁻²)	29.3	N/A
θ_a (rad \AA^{-1})	0.927	N/A
θ_b (rad \AA^{-2})	-1.361	N/A
θ_c (rad)	1.303	N/A
σ_O (\AA)	3.16	3.52
ε_O (kcal/mol)	0.18	0.1825
σ_H (\AA)	0	0.0
ε_H (kcal/mol)	0	0.0
polarizability	1.444	3.34
q_H (e)	eq 6	0.2
q_O (e)	eq 6	-1.2

interfacial thermodynamic properties. Moreover, while for the hydronium cation, polarizability may not be of great importance, for the hydroxide anion, as has been found for other anions,³⁰ its polarizability is expected to be significantly higher and may play a key role in understanding its interfacial properties.

The work presented in this paper is a combination of two different computational approaches for the understanding of the propensity of the hydroxide anion for the air–water interface. The first is using classical molecular dynamics (MD) simulations with polarizable interaction potentials, with a hydroxide anion refined against thermodynamic and structural data. The second is using a newly developed MS-EVB model, which allows for explicit sharing of protons in aqueous solution. For both, the free-energy difference between the aqueous bulk and air–water interface has been calculated for a single hydroxide ion in water. The paper is organized as follows. Section II provides information for the molecular models used, section III gives the Simulation Details, and section IV gives the Results and Discussion using the two methods. Finally, section V gives the Conclusions. For the MS-EVB model, Supporting Information gives some additional details of the parameters and functional forms used for the molecular model.

II. Molecular Model Details

II.A. Classical Simulations. The rigid Dang–Chang water model was utilized for the classical simulations, which has four sites with a Lennard-Jones (LJ) interaction site located on the oxygen atomic position, two partial positive charges on the hydrogen atomic positions, and an m -site located along the oxygen–hydrogen bisector including a partial negative charge and a point polarizability. The potential parameters and the ability to reproduce experimental properties are given in the referenced work.³¹ The classical polarizable hydroxide model, developed for this work, was rigid with two sites. The OH bond length was set to 0.96966 \AA , with a single LJ site located on the oxygen atomic position and charges located on the hydrogen and oxygen atomic positions. The values for these (LJ site and charges) are the same as those used for the MS-EVB model, given in Table 1. A single-point polarizability was used for the classical model, located on the oxygen atomic position, with a value of 2.30 \AA^3 .

II.B. Flexible Water Model. A four-site flexible and polarizable water model was developed for this work since a flexible water model is required to implement the MS-EVB procedure. The model has a single oxygen site, two hydrogen

sites, and an m -site located along the oxygen–hydrogen bisector. An important aspect of water models for interfacial systems is their ability to reproduce the correct intramolecular geometry. The actual interfacial geometry is unknown, but the bulk and gas-phase geometries can be measured experimentally. If a model can represent both the bulk and gas-phase geometries correctly, the probability that their interfacial geometry would be correct would be higher than that if not. One model that correctly reproduces both of these has been developed previously,³² which was fit to reproduce high-level ab initio cluster data. However, to reproduce the proper liquid properties requires the inclusion of nuclear quantum effects, using a technique such as centroid molecular dynamics,³³ which significantly increases the computational cost of the simulations. Since the polarizable MS-EVB model requires significant computational expense in the first place, we deemed it beneficial to develop an empirical water model that does a reasonable job without the need for considering nuclear quantum effects explicitly.

A Morse potential was used to account for bond stretching, in which the two oxygen–hydrogen bond stretches were coupled.

$$U_{\text{Bond}} = D_0[1 - e^{-\alpha(r_1 - r_{0,1})}]^2 + D_0[1 - e^{-\alpha(r_2 - r_{0,2})}]^2 \quad (1)$$

where $r_{0,1}$ and $r_{0,2}$ are given by

$$\begin{aligned} r_{0,1} &= 0.91656 + 0.01159r_2 \\ r_{0,2} &= 0.91656 + 0.01159r_1 \end{aligned} \quad (2)$$

where r_1 and r_2 represent the distances between each hydrogen and the oxygen. It should be emphasized that for r_1 , its equilibrium bond length is dependent on r_2 , and vice versa. The values for α and D_0 are given in Table 1. These were fit to reproduce the symmetric and antisymmetric stretches for the gas-phase IR spectroscopy of water. A bond-bending potential was developed that couples the HOH bond angle with both of the OH bond lengths

$$U_{\text{Bend}} = \frac{k_0}{2}(\theta - \theta_0)^2 \quad (3)$$

$$k_0 = k_a(r_1 - r_2) + k_b r_1 r_2 + k_c \quad (4)$$

$$\theta_0 = \theta_a(r_1 - r_2) + \theta_b r_1 r_2 + \theta_c \quad (5)$$

where the constants k_a and θ_a and the other similar ones are given in Table 1. The values for these constants were fit to reproduce ab initio calculations.³⁴ The gas-phase IR spectroscopy of water was calculated for this model, giving peaks at 1595, 3610, and 3710 cm^{-1} , which agree reasonably with the experimental values of 1595, 3657, and 3756 cm^{-1} .³⁵

When a water molecule is solvated, its bend angle increases, but for traditional molecular mechanics force fields, the opposite occurs; it decreases. To remedy this, the charge distribution can be coupled with the intramolecular geometry.³² For the developed water model, a simple coupling function is used, in which each hydrogen charge is linearly dependent on its OH distance and HOH angle

$$q_H = -0.14r_{\text{OH}} + 0.17\theta_{\text{HOH}} + 0.36 \quad (6)$$

where θ is in radians, and the opposing charge is located on the m -site, which adjusts so the water molecule charge is neutral. At the equilibrium gas-phase geometry ($r = 0.9572$ \AA and $\theta = 104.52^\circ$),³⁶ the hydrogen charge is 0.537 e. This equation was parametrized to give the correct average liquid-phase OH bond length (0.97 \AA) and HOH bend angle (106.1 $^\circ$),³⁷ along with the correct gas-phase values.

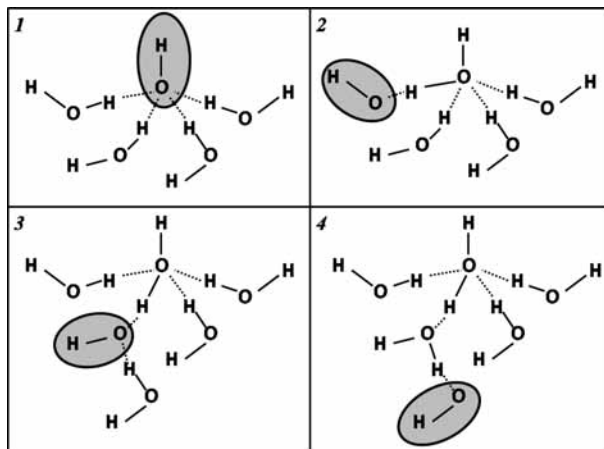


Figure 1. Schematic of the formation of four possible EVB states.

To account for van der Waals interactions, a single Lennard-Jones 12–6 site is located on the oxygen atomic position

$$U_{\text{LJ}} = 4\epsilon \left[\left(\frac{\sigma}{r} \right)^{12} - \left(\frac{\sigma}{r} \right)^6 \right] \quad (7)$$

where the σ and ϵ values are given in Table 1. In addition, there is a single-point polarizability of 1.444 \AA^3 located on the m -site. The m -site itself is dependent on the flexible molecular geometry, with its position defined by the oxygen and the two hydrogen positions

$$x_m = \gamma(x_{\text{H}_1} + x_{\text{H}_2}) + (1 - 2\gamma)x_{\text{O}} \quad (8)$$

where the value for γ was set to 0.192. With this value, the gas-phase dipole for water is 1.85 D.

When polarizability was combined with a four-site flexible water molecule, we found that the polarization catastrophe occurred, and as a result, we used a damping potential for electrostatic interactions as described by Thole and other subsequent work.^{38,39} In essence, at short distances, the charge–charge, charge–dipole, and dipole–dipole interactions are damped. The specific implementation of this closely resembles that of a previously developed water model⁴⁰ and is given in the Supporting Information.

II.C. OH[−] MS-EVB Model. For a classical hydroxide anion in water, multiple water molecules donate a hydrogen bond to the hydroxide oxygen, but no explicit proton sharing is included. In contrast, the MS-EVB model allows these water hydrogens to be shared with the hydroxide anion, with each representing an individual EVB state. The Hamiltonian for the MS-EVB approach is given by

$$H_{\text{EVB}} = \sum_{i=0}^{N_s-1} \sum_{j=0}^{N_s-1} \langle i | \hat{H} | j \rangle \quad (9)$$

where the summation is over all possible EVB states. Each value i corresponds to a different adjacent oxygen–hydrogen pair, which represents the hydroxide anion for the specific EVB state. For illustration, Figure 1 gives an example of the implementation of the MS-EVB technique for a small cluster. While four EVB states are shown in the cluster, many more are possible. The first one is with the defect on the hydroxide anion itself. For the other EVB states, the defect resides on one of the water molecules, and the original hydroxide is treated as a water molecule. These additional EVB states include waters with their hydrogens binding with the hydroxide oxygen (as shown in states 2 and 3 in Figure 1). The criteria for binding are a $\text{O}_{\text{OH}}\text{--H}_w$ distance less than 2.4 \AA and a $\text{H}_{\text{OH}}\text{--O}_{\text{OH}}\text{--H}_w$ angle

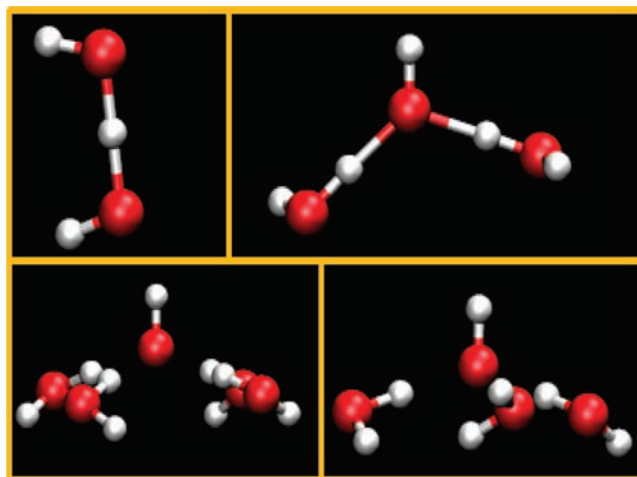


Figure 2. Snapshots of the clusters used to parametrize the MS-EVB hydroxide model. Each has a single hydroxide anion at the top of each figure, along with, in a clockwise fashion, one, two, three, and four waters.

greater than 90° . In addition, waters with hydrogens binding to the first solvation shell water molecules are included in the EVB states, as shown in state 4 in Figure 1. In liquid water, a typical number of EVB states is often around 13.

The described Hamiltonian shown in eq 9 (with N_s EVB states) forms a square matrix with a size of N_s . Diagonal terms are the classical interaction energies using a hydroxide potential (described later) along with the water potential described previously. For each diagonal term, the defect is placed from one oxygen–hydrogen pair to another to coincide with the EVB states, as shown in Figure 1. In addition to these diagonal terms, nondiagonal terms exist, which are parametrized to reproduce ab initio calculations. To determine the energy, the lowest eigenvalue for this matrix is evaluated, and the Hellman–Feynman theorem is used to calculate the forces. Further detailed information on the general implementation of the MS-EVB model can be found in other sources.^{28,29}

Diagonal Terms. As stated earlier, the diagonal terms are calculated with a classical polarizable potential for the hydroxide anion along with the described water model. The hydroxide model nonbonded interactions are similar to those for the classical simulations and are given in Table 1. In addition, a single isotropic point polarizability of 3.34 \AA^3 is located at its oxygen position. This value was calculated from ab initio calculations of an isolated hydroxide anion at the CCSD(T) level, with the aug-cc-pvtz basis set using the Molpro computational package.⁴¹ Unlike the model used for the classical simulations, the hydroxide model here was flexible with a Morse potential fit to represent the OH stretching potential fit from CCSD(T) calculations with the aug-cc-pvtz basis set using the Molpro computational package.⁴¹ Furthermore, Thole damping was used, which is described in the Supporting Information.

Nondiagonal Terms. The nondiagonal terms are used to link two EVB states that share the same hydrogen. This was originally fit to reproduce the potential energy surface of one hydroxide and one water, shown in the upper-left panel of Figure 2, calculated from CCSD(T), with the aug-cc-pvtz basis set using the Molpro computational package.⁴¹ Multiple energy minimizations were carried out, and for each, the oxygen–oxygen distance (r_{OO}) was fixed, along with the q coordinate, which is defined as $q = r_{\text{OO}}/2 - [r_{\text{OH}}]_{\text{OO}}$. The $[r_{\text{OH}}]_{\text{OO}}$ value is defined as the distance between an oxygen and the shared hydrogen projected along the oxygen–oxygen vector. For the water–

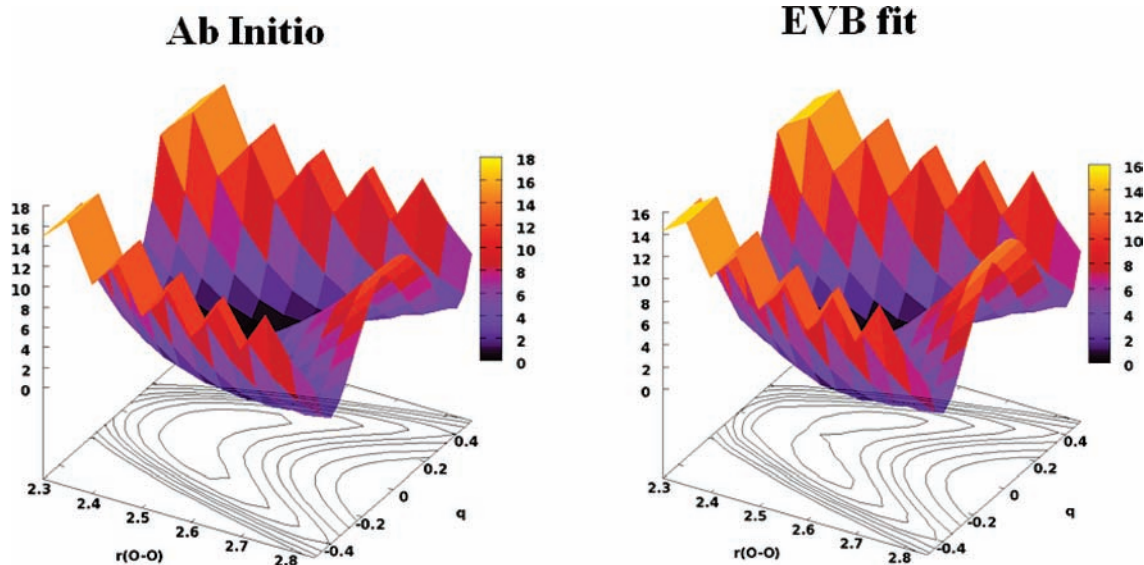


Figure 3. Potential energy surface for a single hydroxide and water molecule from ab initio calculations (left) and the EVB fit (right). The vertical axis and contours represent the energy in kcal/mol offset by -28.0 kcal/mol, and $q = r_{\text{OO}}/2 - [r_{\text{OH}}]_{\text{OO}}$ (as described in the text). Each contour line represents a 1 kcal/mol difference.

hydroxide clusters, there are two EVB states, one placing the defect on the left and the other placing it on the right. A 2×2 MS-EVB matrix is formed with the diagonal terms (1,1 and 2,2) being represented by classical polarizable potentials. The nondiagonal terms are fit so that the total MS-EVB energy reproduces the ab initio potential energy surface (PES). A function that is tanh with respect to r_{OO} and quadratic with respect to q was sufficient to reproduce the ab initio PES. The specific functional form and the parameters used for the fit are given in the Supporting Information. The PES calculated from ab initio results and the EVB fit are given in Figure 3. A reasonably good fit of the ab initio PES was achieved, as is apparent by the agreement between the diagrams.

The PES derived only from the water–hydroxide pair was found to be insufficient to describe cases where multiple waters were bound to a hydroxide anion. To remedy this, the nondiagonal terms also included a contribution due to the angles they had with other water molecules bound to the same hydroxide anion. For instance, consider the upper right panel in Figure 2, which has two waters binding with a hydroxide anion. This would include three EVB states, the first placing the defect on the top (with its hydrogen pointing up), one with the defect on the left (state 2), and one with it on the right (state 3), creating a three-state MS-EVB matrix. The nonzero nondiagonal terms would have i,j values of 1,2 and 1,3 since state 1 is coupled to both states 2 and 3 (but 2 and 3 are not coupled). These nondiagonal terms first include contributions used to derive the PES in Figure 3 but have another term corresponding to the angle between the $\text{O}_3\text{--O}_1\text{--O}_2$ (with O_1 representing the top oxygen) atoms. This second angular term results in a significant increase in the average angle between adjacent water molecules bound to a hydroxide in the minimized structure. The functional form of this is tanh and is given, along with the parameters used, in the Supporting Information. For clusters of size three and four, the angular parameters (but not the functional form) are different. As a result, three separate angular functions were parametrized to correspond with a hydroxide with two, three, and four water molecules bound to it. In rare cases when more than four waters are bound to a hydroxide, the angular term is the same as that with four. These angular potentials were fit to B3LYP DFT cluster calculations with the aug-cc-pvdz basis set.

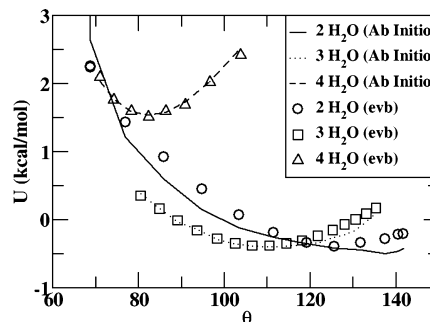


Figure 4. Comparison of the energy dependence for one set of water oxygen–hydroxide oxygen–water oxygen angles between ab initio and the EVB potential for hydroxide clusters with waters. The energies are offset by 50, 70, and 90 kcal/mol for 2, 3, and 4 H_2O , respectively.

It has been shown recently that B3LYP DFT gives similar results as MP2 calculations for hydroxide–water clusters;⁴² therefore, this lower level of theory was deemed adequate for the larger cluster fits. For these calculations, the NWChem computational package was used.^{43,44}

The angular fits made with respect to energy along with the ab initio counterparts are given in Figure 4. The angle in this case corresponds with one $\text{O}_i\text{--O}_1\text{--O}_j$ set, where 1 is the oxygen on the top in the snapshots in Figure 2 and i and j are any two water oxygens bound with the top oxygen. The agreement is reasonable between the fit and the ab initio data. In addition, the dependence of energy on distance for one water oxygen–hydroxide oxygen pair is given in Figure 5 for the MS-EVB model and ab initio data, showing reasonable agreement, even though the distance dependence of these clusters was not specifically fit.

Finally, there were tanh switching functions implemented for the nondiagonal terms. Basically, when an $\text{O}_{\text{OH}}\text{--H}_{\text{Water}}$ distance approached 2.4 \AA or the $\text{H}_{\text{OH}}\text{--O}_{\text{OH}}\text{--H}_{\text{Water}}$ angle approached 90° , the nondiagonal term went to 0. The specific forms of the switching functions are given in the Supporting Information. It should also be noted that the second angular term between oxygens was also coupled to the switching functions. This

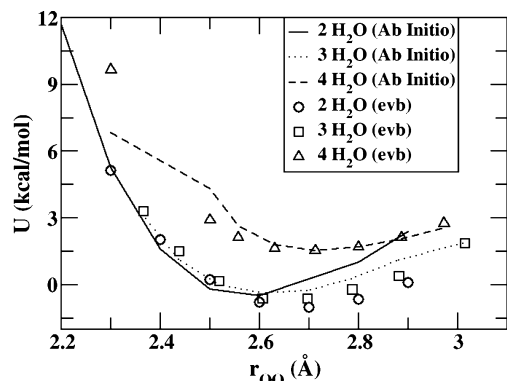


Figure 5. Comparison of the energy dependence of one water oxygen-hydroxide oxygen distance between ab initio and the MS-EVB potential for hydroxide clusters with waters. The energies are offset by 50, 70, and 90 kcal/mol for 2, 3, and 4 H₂O, respectively.

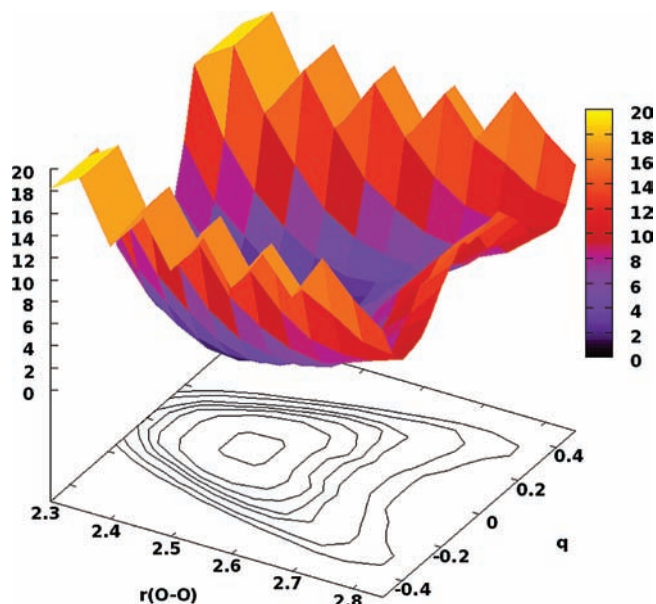


Figure 6. Potential energy surface for a single hydroxide and water molecule with the inclusion of NQE. The axis and contours are defined the same as in Figure 3.

allowed smooth transitions for the oxygen angular term when the number of water oxygens bound to a hydroxide oxygen changed.

Nuclear Quantum Effects. Nuclear quantum effects (NQE) play an important role in the dynamics of proton transport for the hydroxide anion in solution.²⁵ Centroid molecular dynamics³³ can be used to account for nuclear quantum effects and has been used to study proton transport for the hydronium ion.²⁸ However, this results in a significant increase in computational cost, and another solution was desired for this work. One approach used for understanding the hydronium ion was to refit the MS-EVB potential into an effective potential to account for NQE.^{29,45} This method allows NQE to be included implicitly in the potential and does not increase the computational cost of the simulations. The procedure to parametrize the potential is to numerically solve the Feynman path integral⁴⁶ (at 298 K) for the probability distribution of the centroid for each of the r_{OO} and q coordinates.⁴⁷ The form of the integral is given in eq 7 in ref 29. The refit potential is given in Figure 6 and is moderately different than the pure ab initio result, which was also found when NQE was introduced for the hydronium ion.^{29,45} The extra angular contribution (to account for cases when more than one water was bound to a hydroxide) to the MS-EVB potential was not

refit to include NQE since it was based on the heavier oxygen atomic positions and not the hydrogen positions. It should be noted, though, that the angular terms were different for the NQE simulations than those without NQE by a constant offset to give similar binding energies as the ab initio results.

III. Simulation Details

III.A. Classical Simulations. A cubic box of dimensions 26.22 Å in each direction was used for the classical simulations, and 600 water molecules were present. There was a 0.5 ns equilibration period of the system, followed by a 0.5 ns period in which the radial distribution functions were collected. After this period, the z -axis was elongated to 75 Å, allowing two air-water interfaces to form that were normal to the xy plane, followed by another 0.5 ns of equilibration. Finally, the potential of mean force (PMF) technique was used to calculate the free-energy profile of the hydroxide anion across the air-water interface. This technique is described in detail elsewhere^{48,49} and fixes the hydroxide anion center of mass z -coordinate with respect to the liquid center of mass in 1 Å increments across the air-water interface. For each of these positions, an additional 0.5 ns of equilibration was performed, followed by 1.5 ns of production at each position to acquire the average force acting on the hydroxide center of mass along the z -axis. The average force could then be integrated over the z -positions to give a free-energy profile.^{48,49} A question may arise as to if the equilibration time is long enough to converge the force. For the classical hydroxide anion system at the air-water interface with its z -coordinate fixed, we found that the force autocorrelation function converged to 0 in all three dimensions in 0.05 ± 0.02 ps. This is consistent with previous work on ethanol, in which the force autocorrelation function acting along the z -axis at the air-water interface converged to 0 after 0.1–0.2 ps.⁵⁰ These are much shorter than the equilibration time.

III.B. MS-EVB Simulations. MD simulations were carried out using the RESPA algorithm, which allows for the use of multiple time steps.⁵¹ For all simulations, the fast time step was set to 0.02 fs, which included all intramolecular interactions. However, as described in section II.B, the water bond lengths and angles were coupled with the partial charges. The partial charges affect nonbonded interactions (in the Coulomb potential); therefore, there is an effective coupling of the fast intramolecular coordinate with the nonbonded interactions. To remedy this to a degree, the chain rule was applied to split up the energy derivative into fast and slow parts. For instance, the energy derivative with respect to the bond length was evaluated as follows

$$\frac{dU}{dr} = \frac{dU}{dq} \cdot \frac{dq}{dr} \quad (10)$$

where the left derivative was evaluated in the slow time step and the right was evaluated in the fast time step. However, even after splitting up the derivative, a relatively short time step of 0.2 fs was still required for the nonbonded interactions to conserve energy in the MD simulation. When the MS-EVB potential was implemented, all nondiagonal terms and intramolecular diagonal terms were evaluated in the 0.02 fs time step, while the electrostatic and LJ interactions were evaluated in the 0.2 fs time step.

The temperature was set using the Nosé-Hoover chains thermostat, with one chain placed on each atom.⁵² When constant pressure was desired, it was controlled with the Berendsen thermostat.⁵³ Two types of simulations were carried out, bulk simulations, which included 442 water molecules in

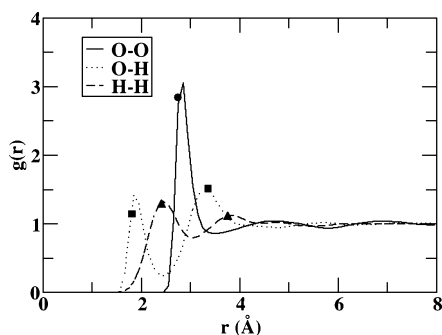
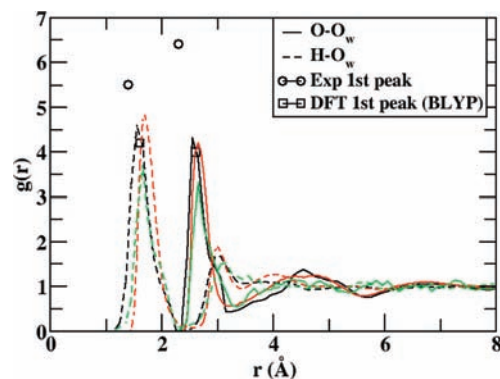
TABLE 2: Comparison of Properties Between Simulation and Experiment at 298 K

property	simulation	experiment
dielec. constant	85 ± 10	78.3 ⁶⁴
ρ_{liquid}	0.995 ± 0.003 g/mL	0.995 g/mL ⁶⁵
ΔH_{vap}	9.95 ± 0.05 kcal/mol	10.5 kcal/mol ⁶⁶
diff. coefficient	2.5 ± 0.2 m ² /s	2.3 m ² /s ⁶⁷
surf. tens.	57 ± 8 dyn/cm	72 dyn/cm ⁶⁸

a cubic box, and interfacial simulations, which were in a slab geometry, with the box length elongated in the z -direction forming two air–water interfaces bisecting the z -axis. These interfacial simulations had dimensions of $22 \times 22 \times 60 \text{ \AA}$, with the liquid length (in the z -direction) being approximately 27 \AA (with the rest being vapor). Simulations with similar setups have been described in detail previously.^{31,54} When hydroxide was present, a single hydroxide anion was included in the simulations, along with 442 water molecules.

IV. Results and Discussion

IV.A. Flexible Pure Water. MD simulations of 1 ns in length in a cubic box with 442 water molecules in the NPT ensemble at 1 atm and 298 K were used to calculate the dielectric constant, liquid density, and heat of vaporization of pure water. The pressure was kept constant with the Berendsen thermostat.⁵³ The heat of vaporization was calculated by taking the difference between the energy per mole in the liquid phase and the gas phase and adding RT to account for the PV term. In addition, the diffusion coefficient was calculated from a 1 ns simulation in the NVE ensemble for the system of 442 water molecules at a density of 0.995 g/mL. It should be noted that this density was set to the average density calculated from the NPT ensemble simulation, and the initial temperature was 298 K, which did not vary significantly during the NVE simulation. To calculate the surface tension, a different simulation setup was used, in which 1000 water molecules were placed in a rectangular box with an elongated z -axis, with respect to the x - and y -axis, forming two air–water interfaces. A 1 ns simulation was carried out, and the surface tension was calculated in the usual way³¹ in the NVT ensemble at 298K. The simulation results for these properties and their comparison with experiment are given in Table 2. Agreement is very good for diffusion, liquid density, and dielectric constant. However, the heat of vaporization and surface tension are somewhat underpredicted with respect to experiment. From the NPT simulations, the radial distribution function (RDF) for the water model was also calculated and is given in Figure 7. The agreement between experiment and simulation is reasonable, but the first OH and OO peaks are at slightly lower distances than those experimen-

**Figure 7.** Comparison of water RDFs between simulation (lines) and experiment⁶⁹ (symbols represent first peak positions).**Figure 8.** Comparison of water RDFs between the MS-EVB simulations with NQE (black lines) and those without NQE (green lines), classical simulations (red lines), experiment,⁷⁰ and AIMD simulations²⁵ (symbols represent first peak positions).

tally. One property of interest that cannot be compared with experiment, and, to the knowledge of the authors, that has not been calculated previously, is the water bend angle at the air–water interface. The value of the HOH water bend angle at the Gibbs dividing surface (GDS) was found to be the same as that in the bulk. Only at values greater than 2 \AA from the GDS (toward the vapor) did the bend angle decrease toward the gas-phase value (not shown).

IV.B. MS-EVB and Classical Hydroxide Anion Simulations. NVE Simulations. Using the MS-EVB model with NQE, six independent 50 ps simulations were carried out in the NVE ensemble to understand the structure of water molecules surrounding the hydroxide anion and to calculate its diffusion coefficient. The initial temperatures and pressures were 298 K and 1 atm, and the actual average temperatures and pressures from these simulations were 302 K and 1.02 atm, slightly different due to drift. The value calculated was $0.21 \pm 0.04 \text{ \AA}^2 \text{ ps}^{-1}$, which compares with the experimental value of 0.53.⁵⁵ This shows that the values predicted from the simulations are underestimated with respect to experiment, likely due to a barrier to proton transfer that is too high. The comparison between the distance dependence of the potential energy between ab initio and the MS-EVB model given in Figure 5 shows that for the four-coordinated hydroxide, the MS-EVB model somewhat overpredicts the potential energy at very short distances. In addition, Figure 8 gives the RDFs, which were calculated from these simulations and compared with the MS-EVB simulations without NQE, classical simulation results, experiment, and AIMD results. Experiment shows a slightly shorter first peak for both the O–O_w and H–O_w peaks, and the peak heights are somewhat higher experimentally. Interestingly, there is little difference in the first peak location and size between the MS-EVB-NQE and AIMD simulations. The most significant difference between MS-EVB-NQE and classical RDFs is that the first H–O_w peak is somewhat broader and at shorter values for the MS-EVB simulation. This is likely due to the proton sharing that only the MS-EVB and AIMD models allow. Furthermore, it can be observed that for the MS-EVB models, the inclusion of NQE allows for shorter H–O_w and O–O_w distances than those without and brings the RDFs closer to the experimental values. This shows that including NQE can be very important for understanding structural properties for this system.

Extracted from the MS-EVB-NQE simulations in the NVE ensemble was the free energy along the γ coordinate,²⁵ which is defined as

$$\gamma = r_{\text{O}^*\text{H}} - r_{\text{OH}} \quad (11)$$

where $r_{\text{O}^*\text{H}}$ is the distance between the shared proton and the hydroxide anion and r_{OH} is the distance between the shared proton and the water molecule that is closest to the hydroxide anion. This value will approach 0 during a proton exchange. During the NVE simulations, the probability distribution was recorded as a function of γ ($P(\gamma)$) and transformed into the free-energy profile ($W(\gamma) = -RT \ln[P(\gamma)]$) given in Figure 9. This was not calculated for the classical simulations since proton-transfer events are not allowed. Using this, a free-energy barrier to proton transfer of 2.3–2.4 kcal/mol was calculated. A direct comparison with experiment is difficult to make, but the experimental energy of activation is approximately 2.5 kcal/mol,⁵⁶ which is similar to the results here.

A snapshot of the waters in the MS-EVB states are given in Figure 10, with the hydroxide oxygen colored yellow for clarity. What is apparent is that there is a strong tetrahedrally coordinated hydroxide anion, which has been found in some AIMD simulations²⁵ but not in others.^{26,27} An interesting feature that is shown in the snapshot is that water molecules that share protons with the hydroxide can often be found above the hydroxide anion (if it is pointed with its hydrogen up) and not just in the region below it.

Interfacial Simulations. The procedure for mapping out a free-energy profile for a classical molecule (described in section

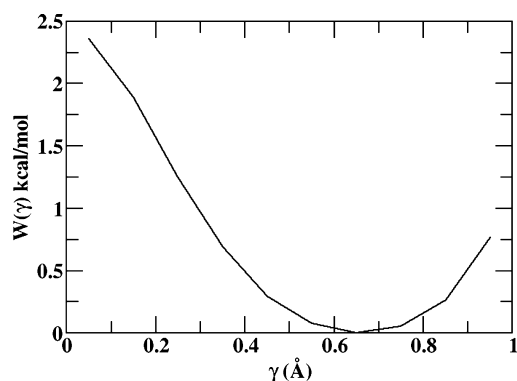


Figure 9. Free-energy profile along the proton reaction coordinate taken from the MS-EVB simulations.

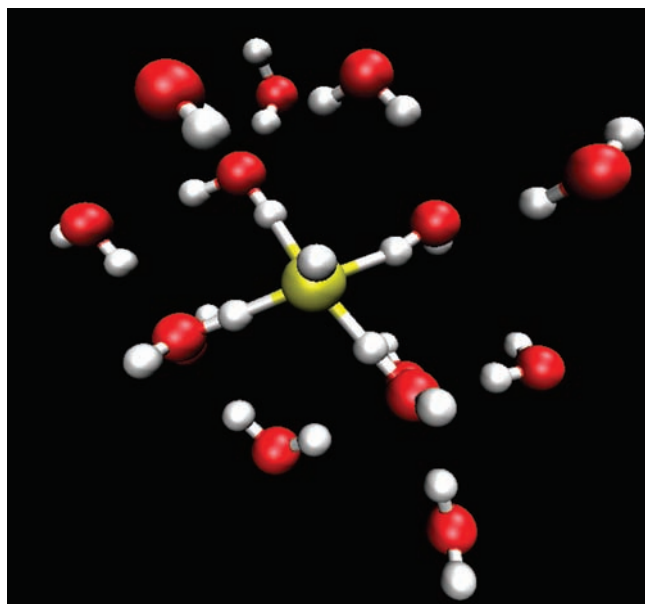


Figure 10. Snapshot showing all possible EVB states for a hydroxide anion in solution.

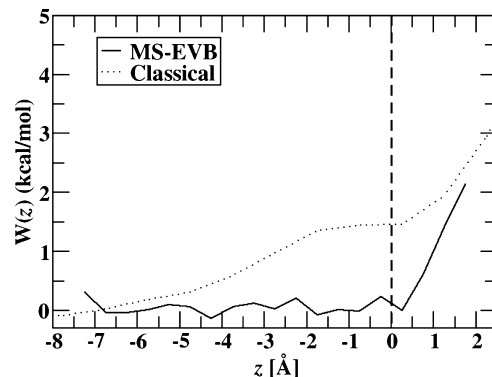


Figure 11. Free-energy profile for the hydroxide anion with respect to GDS (which is 0) of water, with negative values corresponding to the water bulk and positive values corresponding the vapor phase.

III.A) across the air–water has been carried out numerous times and is reasonably well established.^{22,48,57–60} However, for the MS-EVB potential, a constrained coordinate approach (which was used for the classical model) cannot be used due to the fact that a proton-transfer event can occur, causing the hydroxide oxygen to move. To overcome this, umbrella sampling was used in its place,⁶¹ in which a harmonic potential was used for the umbrella potential

$$u(z) = k_z(z_{\text{OH}} - z_0) \quad (12)$$

where k_z was set to 2 kcal/mol for all cases, z_{OH} was the hydroxide anion center of mass, and multiple values of z_0 were used. A total of seven values of z_0 were used, including 0, -1 , -2 , -3 , -4 , -5 , and -6 Å with respect to the GDS of the air–water interface. The GDS was determined by fitting the water density to a hyperbolic tangent function, as has been done previously.³¹ For each case (or z_0 value), two independent 100 ps simulations were carried out, giving 200 ps of total time at each value. The probability distribution for z_{OH} was recorded (corrected for the fact that the umbrella potential was used in the usually way)⁶¹ for each of the simulations, and they were matched in overlapping regions of different z_0 values to give a probability profile with respect to z_{OH} . The probability distribution ($P(z)$) was transformed into a free energy ($W(z) = -RT \ln[P(z)]$). It should be noted that while the hydroxide center of mass was a parameter in the umbrella potential, the potential was applied for each MS-EVB state. The value of $W(z)$ extracted only covers the location of the hydroxide in the state with the lowest eigenvalue of the MS-EVB potential, but the actual umbrella potential influences all MS-EVB states and samples z positions that can be different than the z value shown for $W(z)$. This is illustrated in the snapshot in Figure 10, in which many of the water molecules sharing a hydrogen with the hydroxide anion are located above the hydroxide anion (if up is defined as the direction that its hydrogen is facing). As a result, when the z_0 value is at the GDS itself, the hydroxide anion with the lowest eigenvalue may be well solvated.

Figure 11 gives the free-energy profile calculated from the classical and MS-EVB simulations. The uncertainty for the MS-EVB values was around 0.3 kcal/mol, and it was around 0.1 kcal/mol for the classical model. The classical model shows a clear increase in free energy as the hydroxide anion approaches the GDS. The degree of the free-energy increase may be expected to be sharper as the ion crosses the GDS since the hydration free energy for the hydroxide anion is -105.0 kcal/mol.⁶² However, it should be noted that water molecules are “dragged” with the hydroxide anion (as has been observed for other ions),⁴⁸ and this mitigates

the expected sharp free-energy increase. In contrast, the MS-EVB model shows that the hydroxide anion approaches the GDS with little change in free energy but sharply increases as it crosses it. The molecular configuration of the interfacial hydroxide anions was with the oxygen fully solvated but with its hydrogen pointing toward the vapor without any waters near the hydrogen. This suggests a hydroxide anion that is present at the air–water interface but repelled from its outer edge (or far toward the vapor). A similar conclusion was reached for the propensity of the hydroxide anion for the interface between water and a thermal wall using a classical force field.¹⁶ As a result, there should be some spectroscopic evidence of the hydroxide anion near the air–water interface but not in high concentrations, which has been found experimentally.^{4,14}

The apparent reason that the MS-EVB model has a lower surface free energy than the classical model is due to its tetrahedrally coordinated water molecules. The MS-EVB model enforces that waters only bind if the $H_{OH}-O_{OH}-H_w$ angle is greater than 90° since that is what is found from the *ab initio* calculations. With this, if the hydroxide anion is pointing its hydrogen toward the vapor, it will be fully solvated when the oxygen is at the air–water interface. Previous work has found that for classical hydroxide anion models in bulk water, waters are often found binding with the hydroxide with a $H_{OH}-O_{OH}-H_w$ angle less than 90° .⁶³ As a result, classical models lose some of their solvation if the oxygen is at the air–water interface, reducing its propensity for the air–water interface.

V. Conclusions

Molecular dynamics simulations were carried out utilizing classical and MS-EVB interaction potentials that were developed for this work. Furthermore, a flexible water molecule was developed, giving reasonable agreement with experiment for pure water properties. Moreover, similar results were found for the MS-EVB model and some AIMD simulations for certain properties, but experimental structures were somewhat different when comparing the RDFs. The free-energy profile was calculated using the potential of mean force technique for the classical model and umbrella sampling for the MS-EVB potential. While the classical model showed a moderate increase in free energy for the transfer of a hydroxide anion from the bulk to the interface, the MS-EVB model gave a very sharp increase in free energy, but not until the hydroxide crossed the GDS. This points to an interface with the hydroxide anion present, but not with strong adsorption, that is repelled to the outer edge of the air–water interface.

Acknowledgment. Part of this work was supported by the Division of Chemical Sciences, Geosciences and Biosciences, Office of Basic Energy Sciences, U.S. Department of Energy. Battelle operates the Pacific Northwest National Laboratory for the U.S. Department of Energy. In addition, some of the research was funded by the Louisiana Board of Regents Research Competitiveness Subprogram Contract Number 3LEQSF(2008-11)-RD-A-21. The calculations were carried out using the resources from the Louisiana Optical Network Initiative (LONI). Additional computer resources were provided by the Office of Basic Energy Sciences, U.S. Department of Energy. We also thank C. J. Mundy for sharing their AIMD results with us, which also showed that the hydroxide anion has a propensity for the air–water interface.⁷¹

Supporting Information Available: Details of the charge dampening equations and parameters, the MS-EVB potential function, and parameters. This material is available free of charge via the Internet at <http://pubs.acs.org>.

References and Notes

- (1) Marcus, Y. *Ion Solvation*; John Wiley and Sons Ltd.: New York, 1985.
- (2) Petersen, M. K.; Iyengar, S. S.; Day, T. J. F.; Voth, G. A. *J. Phys. Chem. B* **2004**, *108*, 14804–14806.
- (3) Buch, V.; Milet, A.; Vacha, R.; Jungwirth, P.; Devlin, J. P. *Proc. Natl. Acad. Sci. U.S.A.* **2007**, *104*, 7342–7347.
- (4) Tarbuck, T. L.; Ota, S. T.; Richmond, G. L. *J. Am. Chem. Soc.* **2006**, *128*, 14519–14527.
- (5) Petersen, P. B.; Saykally, R. J. *J. Phys. Chem. B* **2005**, *109*, 7976–7980.
- (6) Marinova, K. G.; Alargova, R. G.; Denkov, N. D.; Velev, O. D.; Petsev, D. N.; Ivanov, I. B.; Borwankar, R. P. *Langmuir* **1996**, *12*, 2045.
- (7) Beattie, J. K.; Djerdjev, A. M. *Angew. Chem., Int. Ed.* **2004**, *43*, 3568.
- (8) Takahashi, M. *J. Phys. Chem. B* **2005**, *109*, 21858.
- (9) Healy, T. W.; Fuerstenau, D. W. *J. Colloid Interface Sci.* **2007**, *309*, 183.
- (10) Klijn, J. E.; Stuart, M. C. A.; Scarzello, M.; Wagenaar, A.; Engberts, J. B. F. N. *J. Phys. Chem. B* **2006**, *110*, 21694–21700.
- (11) Pashley, R. M. *J. Phys. Chem. B* **2003**, *107*, 1714–1720.
- (12) Johnsson, M.; Wagenaar, A.; Stuart, M. C. A.; Engberts, J. B. F. N. *Langmuir* **2003**, *19*, 4609–4618.
- (13) Walker, D. S.; Moore, F. G.; Richmond, G. L. *J. Phys. Chem. C* **2007**, *111*, 6103–6112.
- (14) Petersen, P. B.; Saykally, R. J. *Chem. Phys. Lett.* **2008**, *458*, 255.
- (15) Zangi, R.; Engberts, J. B. F. N. *J. Am. Chem. Soc.* **2005**, *127*, 2272–2276.
- (16) Vacha, R.; Zangi, R.; Engberts, J. B. F. N.; Jungwirth, P. *J. Phys. Chem. C* **2008**, *112*, 7689–7692.
- (17) Mucha, M.; Frigato, T.; Levering, L. M.; Allen, H. C.; Tobias, D. J.; Dang, L. X.; Jungwirth, P. *J. Phys. Chem. B* **2005**, *109*, 7617–7623.
- (18) Kudin, K. N.; Car, R. *J. Am. Chem. Soc.* **2008**, *130*, 3915–3919.
- (19) Randles, J. E. B. *Phys. Chem. Liq.* **1977**, *7*, 107–179.
- (20) Petersen, P. B.; Saykally, R. J. *Chem. Phys. Lett.* **2004**, *397*, 51–55.
- (21) Jungwirth, P.; Tobias, D. J. *Chem. Rev.* **2006**, *106*, 1259–1281.
- (22) Chang, T. M.; Dang, L. X. *Chem. Rev.* **2006**, *106*, 1305–1322.
- (23) Gopalakrishnan, S.; Liu, D. F.; Allen, H. C.; Kuo, M.; Shultz, M. J. *Chem. Rev.* **2006**, *106*, 1155–1175.
- (24) Tuckerman, M. E.; Chandra, A.; Marx, D. *Acc. Chem. Res.* **2006**, *39*, 151–158.
- (25) Tuckerman, M. E.; Marx, D.; Parrinello, M. *Nature (London)* **2002**, *417*, 925–929.
- (26) Asthagiri, D.; Pratt, L. R.; Kress, J. D.; Gomez, M. A. *Proc. Natl. Acad. Sci. U.S.A.* **2004**, *101*, 7229–7233.
- (27) Chen, B.; Park, J. M.; Ivanov, I.; Tabacchi, G.; Klein, M. L.; Parrinello, M. *J. Am. Chem. Soc.* **2002**, *124*, 8534–8535.
- (28) Schmitt, U. W.; Voth, G. A. *J. Chem. Phys.* **1999**, *111*, 9361–9381.
- (29) Brancato, G.; Tuckerman, M. E. *J. Chem. Phys.* **2005**, *122*.
- (30) Vrbka, L.; Mucha, M.; Minofar, B.; Jungwirth, P.; Brown, E. C.; Tobias, D. J. *Current Opin. Colloid Interface Sci.* **2004**, *9*, 67–73.
- (31) Dang, L. X.; Chang, T. M. *J. Chem. Phys.* **1997**, *106*, 8149–8159.
- (32) Fanourgakis, G. S.; Xantheas, S. S. *J. Chem. Phys.* **2006**, *124*.
- (33) Cao, J. S.; Voth, G. A. *J. Chem. Phys.* **1994**, *101*, 6168–6183.
- (34) Partridge, H.; Schwenke, D. W. *J. Chem. Phys.* **1997**, *106*, 4618.
- (35) Hertzberg, G. *Electronic Spectra and Electronic Structure of Polyatomic Molecules*; Van Nostrand Reinhold: New York, 1966.
- (36) Benedict, W. S.; Gailar, N.; Plyler, E. K. *J. Chem. Phys.* **1956**, *24*, 1139.
- (37) Maniero, A. L.; Brustolon, M.; Ottaviani, M. F.; Sgarabotto, P.; Greci, L. *Mol. Phys.* **1991**, *73*, 15.
- (38) Thole, B. T. *Chem. Phys.* **1981**, *59*, 341–350.
- (39) Masia, M.; Probst, M.; Rey, R. *J. Chem. Phys.* **2005**, *123*, 1–13.
- (40) Burnham, C. J.; Li, J.; Xantheas, S. S.; Leslie, M. *J. Chem. Phys.* **1999**, *110*, 4566.
- (41) Amos, R. D.; Bernhardsson, A.; Berning, A.; Celani, P.; Cooper, D. L.; Deegan, M. J. O.; Dobbyn, A. J.; Eckert, F.; Hampel, C.; Hetzer, G.; Knowles, P. J.; Korona, T.; Lindh, R.; Lloyd, A. W.; McNicholas, S. J.; Manby, F. R.; Meyer, W.; Mura, M. E.; Nicklass, A.; Palmieri, P.; Pitzer, R.; Rauhut, G.; Schutz, M.; Schumann, U.; Stoll, H.; Stone, A. J.; Tarroni, R.; Thorsteinsson, T.; Werner, H.-J. In *MOLPRO, a package of ab initio programs design*, version 2002.1; Werner, H.-J., Knowles, P. J., Eds.; 2002.
- (42) Pliego, J. R., Jr.; Riveros, J. M. *J. Chem. Phys.* **2000**, *112*, 4045.
- (43) Kendall, R. A.; Apra, E.; Bernholdt, D. E.; Bylaska, E. J.; Dupuis, M.; Fann, G. I.; Harrison, R. J.; Ju, J. L.; Nichols, J. A.; Nieplocha, J.; Straatsma, T. P.; Windus, T. L.; Wong, A. T. *Comput. Phys. Commun.* **2000**, *128*, 260–283.
- (44) Bylaska, E. J.; et al. *NWChem*, a computational chemistry package for parallel computers, version 5.0; 2006.

- (45) Sagnella, D. E.; Tuckerman, M. E. *J. Chem. Phys.* **1998**, *108*, 2073–2083.
- (46) Feynman, R. P.; Hibbs, A. R. *Quantum Mechanics and Path Integrals*; McGraw-Hill: New York, 1965.
- (47) Kleinert, H. *Path Integrals in Quantum Mechanics, Statistics, Polymer Physics and Financial Markets*; World Scientific: River Edge, NJ, 2004.
- (48) Dang, L. X. *J. Phys. Chem. B* **2002**, *106*, 10388–10394.
- (49) Viececi, J.; Roeselova, M.; Potter, N.; Dang, L. X.; Garrett, B. C.; Tobias, D. J. *J. Phys. Chem. B* **2005**, *109*, 15876–15892.
- (50) Taylor, R. S.; Garrett, B. C. *J. Phys. Chem. B* **1999**, *103*, 844–851.
- (51) Tuckerman, M.; Berne, B. J.; Martyna, G. J. *J. Chem. Phys.* **1992**, *97*, 1990–2001.
- (52) Martyna, G. J.; Klein, M. L.; Tuckerman, M. *J. Chem. Phys.* **1992**, *97*, 2635–2643.
- (53) Berendsen, H. J. C.; Postma, J. P. M.; Vangunsteren, W. F.; Dinola, A.; Haak, J. R. *J. Chem. Phys.* **1984**, *81*, 3684–3690.
- (54) Wick, C. D.; Kuo, I. F. W.; Mundy, C. J.; Dang, L. X. *J. Chem. Theory Comput.* **2007**, *3*, 2002–2010.
- (55) Atkins, P.; de Paula, J. *Atkins's Physical Chemistry*, 7th ed.; University Press: Oxford, U.K., 2002.
- (56) Agmon, N. *Chem. Phys. Lett.* **2000**, *319*, 247–252.
- (57) Wick, C. D.; Dang, L. X. *Chem. Phys. Lett.* **2008**, *458*, 1–5.
- (58) Wick, C. D.; Dang, L. X. *J. Chem. Phys.* **2007**, *126*, 134702 (1–4).
- (59) Dang, L. X.; Chang, T. M. *J. Phys. Chem. B* **2002**, *106*, 235–238.
- (60) Wick, C. D.; Dang, L. X. *J. Phys. Chem. B* **2006**, *110*, 8917–8920.
- (61) Torrie, G. M.; Valleau, J. P. *J. Comput. Phys.* **1977**, *23*, 187.
- (62) Pliego, J. R., Jr.; Riveros, J. M. *Phys. Chem. Chem. Phys.* **2002**, *4*, 1622–1627.
- (63) Ufimtsev, I. S.; Kalinichev, A. G.; Martinez, T. J.; Kirkpatrick, R. *J. Chem. Phys. Lett.* **2007**, *442*, 128–133.
- (64) Buchner, R.; Barthel, J.; Stauber, J. *Chem. Phys. Lett.* **1999**, *306*, 57–63.
- (65) Eisenberg, D.; Kauzmann, W. *The Structure and Properties of Water*; Oxford University Press: London, 1969.
- (66) Kell, G. S. *J. Chem. Eng. Data* **1975**, *20*, 97–105.
- (67) Krynicky, K.; Green, C. D.; Sawyer, D. W. *Faraday Discuss. Chem. Soc.* **1978**, *66*, 199–208.
- (68) MacRitchie, F. *Chemistry at Interfaces*; Academic Press: San Diego, CA, 1990.
- (69) Head-Gordon, T.; Hura, G. *Chem. Rev.* **2002**, *102*, 2651–2670.
- (70) Botti, A.; Bruni, F.; Imberti, S.; Ricci, M. A.; Soper, A. K. *J. Chem. Phys.* **2003**, *119*, 5001–5004.
- (71) Mundy, C. J.; Kuo, I.-F. W.; Tuckerman, M. E.; Lee, H.-S.; Tobias, D. J. Submitted for publication.

JP900290Y